NASA Technical Memorandum 86691

Application of Large-Eddy Interaction Model To Channel Flow

S.K. Hong and M.W. Rubesin

February 1985

NASA
National Aeronautics and
Space Administration

NASA Technical Memorandum 86691

Application of Large-Eddy Interaction Model To Channel Flow

S. K. Hong and M. W. Rubesin
Ames Research Center, Moffett Field, California

National Aeronautics and
Space Administration

Ames Research Center
Moffett Field, California 94035

APPLICATION OF LARGE-EDDY INTERACTION MODEL TO CHANNEL FLOW

S. K. Hong* and M. W. Rubesin**
NASA Ames Research Center
Moffett Field, CA 94035

A procedure utilizing an expansion of proper orthogonal functions (or modes) to predict a fully developed flow in channel is derived. To examine numerical and conceptual difficulties, preliminary computations are performed with assigned mean velocity, and turbulence is expressed with only the first mode. The nonlinear interactions of the components of the first mode are treated specifically, with the influence of higher modes neglected; this treatment requires adjustment of the skewness and effective Reynolds number to assure energy equilibrium of the first mode. Computational results show that the first mode possesses the structural character similar to that of the entire flow.

Nomenclature

d = channel half-width

H = channel width

$\vec{k}$ = (k_1, k_3), wave number vector

k = $\sqrt{k_1^2 + k_3^2}$

p = pressure fluctuation

$P_1, \ldots, P_8$ = large-eddy spectra

$\overline{q^2}$ = $\overline{u^2} + \overline{v^2} + \overline{w^2}$, twice of turbulent kinetic energy

Re = Reynolds number

R_{ij} = two-point velocity correlation

S = $\overline{\alpha_1^3}/(\overline{\alpha_1^2})^{3/2}$, skewness parameter

t = tU_o/H, dimensionless time

$\tilde{U}_i$ = instantaneous velocity

U_i = time-averaged velocity

U_o = mean velocity at the channel centerline

u_i = (u,v,w), velocity fluctuation

*NRC Research Associate.
**Senior Staff Scientist.

u^* = wall-friction velocity

$\overline{u_i u_j}$ = Reynolds stress tensor

$\overline{u^2}$ = streamwise turbulent intensity

$\overline{uv}$ = shear stress

$\vec{x}$ = (x,y,z), position vector

Greek Symbols

α_n = random coefficient

λ_n = $\sqrt{\overline{\alpha_n^2}}$, energy of nth mode

ν = kinematic viscosity

ν_T = eddy viscosity

$\pi^{(n)}$ = nth mode of pressure fluctuation

$\phi_i^{(n)}$ = nth mode of velocity fluctuation

Subscripts

i = 1,2, or 3 in streamwise, normal, or spanwise direction, respectively

n = indicates order of mode

Superscripts

1 = indicates first mode

n = indicates nth mode

$(\bar{})$ = ensemble average

$(\,)'$ = differentiation with respect to y

1 Introduction

The mean velocities and the local structure of turbulence under given initial and boundary conditions are subjects of importance in the engineering predictions of inhomogeneous, turbulent shear flows. The most popular prediction methods assume that the Navier-Stokes equations are adequate for describing turbulent flow on an instantaneous basis and are used to develop statistical equations for the various turbulent moments, including the Reynolds stresses. However, the Navier-Stokes equations involve more turbulent moments than there are equations to explain them, forming an unclosed system. Various levels of closure schemes have been proposed: the zero-equation model [1], the two-equation model [2,3], and the Reynolds stress equation model [4,5]. Each of the foregoing methods requires the introduction of several empirical constants with respect to various turbulent processes, and only provides

approximate predictions of the nature of individual turbulent processes arising in a given flow. An approach that examines the dynamics of the turbulence may require less reliance on modeling. Earlier, one of the authors used the Proper Orthogonal Decomposition Theorem (PODT) [6,7] to analyze the structural character of turbulence in boundary layers over variously curved walls [8]. He found that the first mode of the decomposition exhibits the structural character of the averaged turbulence moments quite well even though all the nonlinear effects were modeled in the framework called the Large-Eddy Interaction Model (LEIM) [9-11]. This work suggested that only a few properly identified modes in the decomposition may be needed if the PODT is utilized in a predictive sense and led to the current work.

It should be noted that Lumley's [7] primary purpose was to define unambiguously the meaning of an "eddy." Given two-point velocity correlations from experiments, the PODT has been applied to a pipe flow [12], a wake [13], and a flat-plate boundary layer [14] as a means of extracting the features of a dominant eddy. In a similar approach with the results from a computationally simulated, fully developed channel flow, Moin [15] has specifically investigated as to how many modes are necessary in the PODT to reproduce the turbulent intensities and shear stress. Moin [15] shows that in the case of shear stress it takes the first 15 terms in the series representation before the calculated stress distribution matches the value simulated earlier [16] across the boundary layer. However, when only the wall region is examined, the sum of the first three modes yields the "experimental" results quite well. This small number of modes needed to describe the turbulence gave further encouragement to the authors to extend the PODT approach as a predictive tool as was done in the LEIM.

The basic procedure of the LEIM consists of the following steps: (a) decomposing the velocity fluctuations into orthogonal functions with random coefficients; (b) constructing dynamical equations for those functions; (c) identifying the first mode as an organized structure that contributes most to the energy [7,17]; and (d) evaluating the large eddy which interacts with the mean flow and the eddy-eddy interactions.

In the past, all the nonlinear terms in the LEIM were modeled in a linear form utilizing either an anisotropic eddy viscosity or a diffusion velocity. In this process three empirical constants were introduced in the closure and then determined by matching shapes between normalized Reynolds stresses

calculated from the first mode and experimental measurements. In view of the emphasis of the past applications of the LEIM on evaluating the normalized structure of the first mode, it was primarily a diagnostic method. In the present work to develop a predictive method, the turbulent transport processes have been reexamined and retained in their nonlinear form to minimize the dependence on turbulence modeling and to allow evaluation of the magnitudes of the moments. The applicability of the new transport model has been illustrated in a channel flow that is inhomogeneous in the direction normal to the wall. The computed results shown here are restricted to use of only a single mode in the decomposition and, as stated earlier, this forced the introduction of the skewness and the effective Reynolds number as parameters of the problem. Although the current work has not yet demonstrated the uniqueness of a set of these parameters, results based on different sets of these parameters that satisfy the energy equilibrium of the large eddy yield Reynolds stresses that are less than a few percent apart over the entire channel.

2 Large-Eddy Interaction Model

One can consider a decomposition of the instantaneous velocity, $\tilde{U}_i$, into a time-mean value and its fluctuation as

$$\tilde{U}_i = U_i + u_i \tag{1}$$

where U_i is the time-averaged mean velocity. The velocity fluctuation in equation (1) may be represented as a series in terms of orthogonal functions, $\{\phi_i^{(n)}, n = 1,2,3...\}$, that is

$$u_i(\vec{x},t) = \sum_{n=1}^{\infty} \alpha_n(t)\phi^{(n)}(\vec{x}) \tag{2}$$

Here $\alpha_n(t)$ are random coefficients and uncorrelated from one another, which means

$$\overline{\alpha_m\alpha_n} = \lambda_n^2(t) \cdot \delta_{mn} \tag{3}$$

The overbar, $(\bar{})$, represents an ensemble average. In addition, the $\phi_1^{(n)}$'s are assumed to be orthonormal functions:

$$\int \phi_1^{(p)}\phi_1^{(q)}\, d\vec{x} = \delta_{pq} \tag{4}$$

It then follows [7] that the two-point velocity correlation, R_{ij}, can be expressed with λ_n and $\phi_i^{(n)}$ in the form:

$$R_{ij}(\vec{x},\vec{x}'',t) = \overline{u_i(\vec{x},t)u_j(\vec{x}'',t)}$$

$$= \sum_{n=1}^{\infty} \lambda_n^2 \phi_i^{(n)}(\vec{x}) \cdot \phi_j^{(n)}(\vec{x}'') \qquad (5)$$

Equation (5) implies that if one can predict $(\lambda_n \phi_i^{(n)})$, then various two-point correlations and Reynolds stress components can be calculated directly.

To formulate a framework for $(\lambda_n \phi_i^{(n)})$, we first substitute equation (2) into the Navier-Stokes equation for u_i. After a few manipulations, dynamical equations for the nth mode then become the following under incompressible flow assumptions [7]:

$$\frac{\partial(\lambda_n \phi_i^{(n)})}{\partial t} + U_j \frac{\partial}{\partial x_j}(\lambda_n \phi_i^{(n)}) + \frac{\partial U_i}{\partial x_j}(\lambda_n \phi_j^{(n)})$$

$$+ \frac{\partial}{\partial x_j}\left\{ \sum_{p=1}^{\infty} \sum_{q=1}^{\infty} \frac{\overline{\alpha_n \alpha_p \alpha_q}}{\lambda_n} \phi_i^{(p)} \phi_j^{(q)} \right\}$$

$$= \frac{\partial(\lambda_n \pi^{(n)})}{\partial x_i} + \nu \frac{\partial^2(\lambda_n \phi_i^{(n)})}{\partial x_j \partial x_j}$$

$$(n = 1,2,3, \ldots) \qquad (6)$$

The continuity relationship yields

$$\frac{\partial(\lambda_n \phi_j^{(n)})}{\partial x_j} = 0 \qquad \text{(sum over index } j\text{)} \qquad (7)$$

where $(\lambda_n \pi^{(n)}) = \overline{-\alpha_n p}/\rho$. However, only the system of equations corresponding to $n = 1$ in the above will be considered in the current paper. The index, i, may have values of 1, 2, or 3, corresponding to the streamwise direction (x), the local normal to the wall (y), and the spanwise direction (z), respectively. The nonlinear term appearing in equation (6) when $n = 1$ represents the interaction process between eddies of various order and requires a closure assumption in view of the presence of higher order modes, $\phi_i^{(2)}, \phi_i^{(3)}, \ldots$.

2.1 Transport Process

The nonlinear interaction between the first mode is retained in its original form, but the interactions involving modes higher than $\phi_i^{(1)}$ are modeled. A simple way of accounting for the effect of the higher modes is to group them together and to relate this effect to a known quantity. An eddy viscosity is introduced for this purpose [18,19]:

$$\sum_{p=1}^{\infty}\sum_{q=1}^{\infty}\frac{\overline{\alpha_1\alpha_p\alpha_q}}{\lambda_1}\phi_i^{(p)}\phi_j^{(q)} = \frac{\overline{\alpha_1^3}}{\lambda_1}\phi_i^{(1)}\phi_j^{(1)} - \nu_T\left\{\frac{\partial(\lambda_1\phi_i^{(1)})}{\partial x_j} + \frac{\partial(\lambda_1\phi_j^{(1)})}{\partial x_i}\right\} \tag{8}$$

which has also been suggested by Lumley [7]. In equation (8), ν_T denotes an eddy viscosity. In the present analysis, ν_T is kept equal to a constant, independent of mesh dimensions or the distance from the wall. This has an effect of reducing the effective Reynolds number by a factor of $\nu/(\nu + \nu_T)$. The purpose of the current study is to investigate whether we need to include the effects of higher modes. Although improved models (with variation in the y-direction) are required, in the present preliminary study a constant eddy-viscosity model is incorporated to achieve a steady-state solution. We realize that the computational results indicating the magnitude of the effect of higher modes will be affected by this choice.

Upon substituting equation (8) into (6), one obtains a closed system of equations for $(\lambda_1\phi_i^{(1)})$

$$\frac{\partial}{\partial t}(\lambda_1\phi_i^{(1)}) + U_j\frac{\partial}{\partial x_j}(\lambda_1\phi_i^{(1)}) + \frac{\partial U_i}{\partial x_j}(\lambda_1\phi_j^{(1)}) + S\frac{\partial}{\partial x_j}\{(\lambda_1\phi_i^{(1)})(\lambda_1\phi_j^{(1)})\} = \frac{\partial}{\partial x_i}(\lambda_1\pi^{(1)}) + (\nu + \nu_T)\frac{\partial^2}{\partial x_j\partial x_j}(\lambda_1\phi_i^{(1)}) \tag{9}$$

where $S\ (= \overline{\alpha_1^3}/(\overline{\alpha_1^2})^{3/2})$ is the skewness factor of the random coefficient, α_1. Assuming that the mean velocity is given, the system of equations involves then a structural parameter, S, and a stability parameter, ν_T, which need to be chosen. For the LEIM to be a completely predictive scheme, it requires incorporation of the mean momentum equation for U_i along with

equations (7) and (9). However, for the present, emphasis will be placed on how the large eddy interacts and reacts to a known mean flow field.

3 Application

Fully developed turbulent channel flow is a case for which a large data base has become available over the years. Accordingly, two-dimensional channel flow has been chosen to demonstrate the validity of the approximation for the nonlinear eddy-eddy interaction terms as proposed in equation (8) and to establish the contribution of the first mode to various statistical turbulence quantities. In the fully developed region of the channel, the mean velocity is one-dimensional and is dependent only on the normal coordinate, y, where $y = 0$ corresponds to the lower wall and $y = H$ to the upper wall. Thus, the turbulent flow in the two-dimensional channel flow can be regarded as homogeneous in both streamwise (x) and spanwise (z) coordinates, while strong inhomogeneity is retained in the y-direction. For this case, one can define spectral functions for the first mode of velocity fluctuation, $\lambda_1\phi_i^{(1)}$, and of pressure fluctuation, $\lambda_1\pi^{(1)}$, as follows.

$$\begin{aligned}\hat{\phi}_i(k_1,y,k_3,t) &= \frac{1}{(2\pi)^2}\iint_{-\infty}^{\infty}\{\lambda_1(t)\phi_i^{(1)}(x,y,z)\} \\ &\quad \times \exp\{-\hat{i}(k_1x + k_3z)\}dx\,dz \\ \hat{\pi}(k_1,y,k_3,t) &= \frac{1}{(2\pi)^2}\iint_{-\infty}^{\infty}\{\lambda_1(t)\pi^{(1)}(x,y,z)\} \\ &\quad \times \exp\{-\hat{i}(k_1x + k_3z)\}dx\,dz\end{aligned} \tag{10}$$

where k_1 and k_3 are wave numbers and $\hat{i} = \sqrt{-1}$. The superscript indicating mode (1) is understood in the spectral functions. Applying these definitions into equations (7) and (9), one obtains four complex equations with respect to the large eddy spectra, $\hat{\phi}_i$ ($i = 1,2,3$) and $\hat{\pi}$. These equations can be further divided into eight equations for the real and imaginary parts defined according to the following notation.

$$\begin{aligned}\hat{\phi}_1 &= P_1 + \hat{i}P_2 \\ \hat{\phi}_2 &= P_3 + \hat{i}P_4 \\ \hat{\phi}_3 &= P_5 + \hat{i}P_6 \\ \hat{\pi} &= P_7 + \hat{i}P_8\end{aligned} \tag{11}$$

The nonlinear terms require the convolution theorem [20] during the transformation of the system of equations, equations (7) and (9), into the mixed, (k_1,y,k_3,t), space. The spectral equations become

$$\frac{\partial\hat{\phi}_1}{\partial t} + \hat{i}k_1U\hat{\phi}_1 + U'\hat{\phi}_2 + S \cdot \mathcal{F}\left\{\frac{\partial}{\partial x_j}(\phi_1^{(1)}\phi_j^{(1)})\right\} - \hat{i}k_1\hat{\pi} - (\nu + \nu_T)(\hat{\phi}_1'' - k^2\hat{\phi}_1) = 0 \tag{12}$$

$$\frac{\partial\hat{\phi}_2}{\partial t} + \hat{i}k_1U\hat{\phi}_2 + S \cdot \mathcal{F}\left\{\frac{\partial}{\partial x_j}(\phi_2^{(1)}\phi_j^{(1)})\right\} - \hat{\pi}' - (\nu + \nu_T)(\hat{\phi}_2'' - k^2\hat{\phi}_2) = 0 \tag{13}$$

$$\frac{\partial\hat{\phi}_3}{\partial t} + \hat{i}k_1U\hat{\phi}_3 + S \cdot \mathcal{F}\left\{\frac{\partial}{\partial x_j}(\phi_3^{(1)}\phi_j^{(1)})\right\} - \hat{i}k_3\hat{\pi} - (\nu + \nu_T)(\hat{\phi}_3'' - k^2\hat{\phi}_3) = 0 \tag{14}$$

$$\hat{i}k_1\hat{\phi}_1 + \hat{\phi}_2' + \hat{i}k_3\hat{\phi}_3 = 0 \tag{15}$$

where $(\,)' = d(\,)/dy$ and $k^2 = k_1^2 + k_3^2$. From equations (12)-(14), we denote

$$\mathcal{F}\left\{\frac{\partial}{\partial x_j}(\phi_i^{(1)}\phi_j^{(1)})\right\} = \iint_{-\infty}^{\infty} \hat{i}k_1''\hat{\phi}_i(\vec{k}'')\hat{\phi}_1(\vec{k} - \vec{k}'') + \frac{d\hat{\phi}_i(\vec{k}'')}{dy}\hat{\phi}_2(\vec{k} - \vec{k}'') + \hat{i}k_3''\hat{\phi}_i(\vec{k}'')\hat{\phi}_3(\vec{k} - \vec{k}'')\, dk_1''\, dk_3'' \tag{16}$$

where $\vec{k} = (k_1,k_3)$.

From a consideration of two-point velocity correlations and Reynolds stresses, a relation can be found between the spectra of the double velocity correlations and the $\hat{\phi}_i$'s [21]:

$$\hat{R}_{ij}^{(1)}(k_1'',y,k_3'',t)\delta(\vec{k} + \vec{k}'')$$

$$= \hat{\phi}_i(k_1,y,k_3,t)\hat{\phi}_j(k_1'',y,k_3'',t) \tag{17}$$

where δ is the Dirac delta function and superscript (1) indicates the contribution of the dominant mode. $\hat{R}_{ij}$ is defined in

$$R_{ij}(r_1,y,r_3,t)$$

$$= \iint_{-\infty}^{\infty} \hat{R}_{ij}(k_1,y,k_3,t)\exp\{\hat{i}(k_1r_1 + k_3r_3)\}dk_1\, dk_3 \tag{18}$$

For a flow which is homogeneous in (x,y)-planes:

$$R_{ij}(x,y,z,t;r_1,r_3)$$

$$= \overline{u_i(x,y,z,t)u_j(x + r_1,y,z + r_3,t)}$$

$$= \sum_{n=1}^{\infty} \overline{\alpha_n^2}(t)\phi_i^{(n)}(x,y,z)\phi_j^{(n)}(x + r_1,y,z + r_3)$$

$$\simeq \overline{\alpha_1^2}\phi_i^{(1)}(x,y,z)\phi_j^{(1)}(x + r_1,y,z + r_3) \tag{19}$$

where $\simeq$ indicates simple truncation after the first mode. When $r_1 = r_3 = 0$ in equations (18) and (19), the two-point correlation reduces to the usual Reynolds stress tensor, $\overline{u_iu_j}(y,t)$. Thus, at time t:

$$\overline{u_iu_j}^{(1)}(y,t)$$

$$= \iint_{-\infty}^{\infty} \hat{\phi}_i(k_1,y,k_3,t)\hat{\phi}_j^*(k_1,y,k_3,t)dk_1\, dk_3 \tag{20}$$

where $(\,)^*$ denotes the complex conjugate of $(\,)$. The following structural quantities are also presented: (i) normal stress intensities ($\overline{u_i^2}/\overline{q^2}$), where $\overline{q^2} = \overline{u^2} + \overline{v^2} + \overline{w^2}$; (ii) shear stress intensity ($\overline{uv}/\overline{q^2}$); (iii) orientation of the principal axes of the large eddies (θ), which is given by

$$\theta = (1/2)\tan^{-1}\{-2\overline{uv}/(\overline{u^2} - \overline{v^2})\} \tag{21}$$

and (iv) anisotropy $(\overline{u^2}/\overline{v^2})$.

4 Calculation Procedure

The next objective is to calculate the first mode in the velocity fluctuation expansion and to investigate the extent of the influence of the first mode on the turbulent intensities and the other various structural quantities. Attention is given to the role of the skewness parameter, S, that appears in equation (9), on the solution for the first mode, $\phi_i^{(1)}$, and on the structure of turbulence deduced therefrom.

To solve equations (12)-(15), after one adopts a numerical algorithm he or she needs: (i) initial and boundary conditions, (ii) the local mean velocity profile, and (iii) a proper skewness factor as well as an eddy viscosity. Numerical results of the statistical quantities can then be compared with the classical measurements owing to Laufer [22], for example, from which a particular flow condition is selected as

$$U_o = 7.574 \text{ (m/sec)}$$
$$u^* = 0.2891 \text{ (m/sec)}$$
$$H = 12.7 \text{ (cm)}$$
$$Re = U_o H/\nu = 60380$$

where U_o, u^*, H, and Re are the mean velocity at the channel centerline, wall-friction velocity, channel width, and Reynolds number, respectively.

4.1 Initial and Boundary Conditions

A numerical solution for the large eddy spectra governed by the system of equations (12)-(15) is determined as an initial-boundary value problem in the (y,t) space for various values of wave number, $\vec{k}$. The initialization can be arbitrary because of the goal of achieving a steady solution in the presence of a fixed-mean strain.

At the wall (y = 0), the no-slip condition requires

$$P_1 = P_2 = P_3 = P_4 = P_5 = P_6 = 0 \tag{22}$$

The boundary condition for the pressure spectrum is deduced again from the v component (normal to surface) equation applied at the wall [23]. The spatial derivative for the pressure fluctuation is then discretized using a three-point forward formula beginning at y = 0.

For the other set of boundary conditions, the flow field has been assumed to be symmetric with respect to the centerline (y = H/2), giving

$$P_1' = P_2' = P_5' = P_6' = P_7' = P_8' = 0 \tag{23}$$

$$P_3 = P_4 = 0 \tag{24}$$

where ( )' denotes the derivative with respect to y. It should be pointed out that the entire channel from y = 0 to y = H has been solved in a single instance with the no-slip condition imposed at both ends, y = 0 and y = H. The results show symmetric profiles for u and w spectra and antisymmetric for v spectra (P_3 and P_4), justifying the use of the current boundary conditions at the centerline.

The implicit numerical scheme employed [24] utilizes a two-point backward differencing in time and a three-point central differencing in y. The nonlinear convolution integrals are treated as known by evaluating them at a previous time step when the solution is known. The numerical integration for these terms is carried out employing the trapezoidal rule over the wave number space, (k_1'',k_3''), at a given point, (k_1,y,k_3,t). This enables the formation of a system of matrix equations for all y at each advanced time level, where the coefficient matrix becomes block tridiagonal and diagonally dominant. The inhomogeneous y-coordinate is discretized as suggested by Murphy and Rubesin [25] and the half of the channel is divided by 35 nonuniform grids.

The wave number space, (k_1,k_3), has also been divided into strongly nonuniform meshes. The wave number plane is covered with (17,17) grids where the values are equally spaced in the logarithmic scale for each wave number direction in the range between -10 and 10 (1/cm). It is found (via numerical experimentation) that the wave numbers outside this range have negligible effect on the turbulent stresses.

4.2 Mean Velocity Profile

The mean velocity profile is approximated by a near-wall Prandtl-Taylor model and a blending profile near the center plane.

(i) $U^+ = y^+$ $\qquad (y^+ < 12)$

(ii) $U^+ = 3.0 \ln y^+ + 5.5$ $\qquad (12 \leq y^+ < 760)$

(iii) $U/U_o = 1.0 + 0.068 \log (y/d)$ $\qquad (y^+ \geq 760)$

where $U^+ = U/u^*$, $y^+ = yu^*/\nu$, and $d = H/2$. The mean velocity profile in the outer layer (iii) has been modified in this form for the purpose of matching with the law of the wall (ii) smoothly using the experimental data.

4.3 Effect of Parameters

During the computation, a fairly small time step (normalized by the mean velocity at the channel centerline and by the channel height) of about 0.001 has to be used to ensure numerical stability. Although $\hat{\phi}_i$, governed by equations (12)-(15), can vary in time in any fashion with the current eddy-viscosity model, the fully developed steady-mean flow and boundary conditions used here cause the solution to converge to a steady state. In the current computation, the procedure has been continued up to 200 iterations in time to achieve an accurate asymptotic solution.

5 Results and Discussion

The effect of various values of the parameters, S and ν_T, in equations (12)-(14) on the solution is discussed. After a pair of those values is selected, numerical results obtained in the mixed space (k_1,y,k_3,t) are integrated over the wave number space to yield Reynolds stresses as a function of y. The computed stresses and structural quantities are compared with the experimental data of Laufer [22].

5.1 Determination of Parameters (S and ν_T)

The skewness parameter, S, can be regarded as a structural parameter affecting the anisotropy obtained from the solution, $\hat{\phi}_i$. On the other hand, the primary role of the eddy viscosity, ν_T, is to stabilize the growth of the solution subject to production in a fixed-mean velocity field. We pick a value of S first and then determine corresponding value of ν_T which yields a steady-state solution. One may argue that a choice of a particular set of S and ν_T is not unique on the ground that other combinations of S and ν_T could also produce steady-state results. It has been found, however, that the solution is rather insensitive to the choices of the combinations of S and ν_T that yield steady solutions.

Figure 1 shows the growth of the turbulent kinetic energy, integrated over the channel, for the various values of S as a function of time in the absence of higher modes, $\nu_T = 0$, and for a single case with $\nu_T = 18$. With $\nu_T = 0$, the growth rate increases with increasing S, and it was found for $|S| \geq 0.03$ the solution grows so rapidly that it becomes unstable. However, for $S = 0.01$ and $\nu_T = 18$, the desired steady state in kinetic energy is achieved. Also, for $S = 0.03$ a steady solution for kinetic energy occurs when $\nu_T = 22$.

To examine further whether each component of the kinetic energy has indeed reached a steady state for the above two sets of parameters, each component of the three turbulent intensities is integrated over the channel from $y = 0$ to $y = d$. The results are presented in Fig. 2 as a function of time. It turns out that the u-component energy for $S = 0.01$ and $\nu_T = 18$ maintains a constant value, but that for $S = 0.03$ and $\nu_T = 22$ continues to decrease slightly in Fig. 2. For both cases the w component continues to increase whereas the v component decreases, again at a slow rate. The behavior of these different growth rates can be attributed to the use of an isotropic eddy viscosity in equation (8) and suggests the use of an anisotropic eddy viscosity or some other alternative. Nevertheless, in view of the small growth rate in the v and w components, this behavior is believed to be relatively unimportant so that no attempt was made to eliminate this continually varying anisotropy. The authors favor the case of $S = 0.01$ and $\nu_T = 18$ because it yielded a steady solution slightly better than the other case. However, the calculated Reynolds stresses for these two sets of parameters were well within a few percent of each other (see Table 1 for numerical values of the Reynolds stresses). Thus, the choice of which set to use is not critical to the results shown in the rest of the paper which is based on $S = 0.01$ and $\nu_T = 18$.

5.2 Eddy-Eddy Interactions

Let's write the eddy-eddy interactions affecting the net production of the first mode in the form:

$$\underline{P}(\lambda_1\phi_i^{(1)}) = \underbrace{\frac{\partial U_i}{\partial x_j}(\lambda_1\phi_j^{(1)})}_{\text{"A"}} + \underbrace{S\frac{\partial}{\partial x_j}\{(\lambda_1\phi_i^{(1)})(\lambda\,\phi_j^{(1)})\}}_{\text{"B"}}$$

$$- \nu_T \underbrace{\frac{\partial^2(\lambda_1\phi_i^{(1)})}{\partial x_j \partial x_j}}_{\text{"C"}} \qquad (25)$$

The term "A" governs the interaction with the mean flow. The term "B" corresponds to the transport of the $\phi_i^{(1)}\phi_j^{(1)}$, whereas the term "C" represents the effects of the higher modes modeled by the eddy viscosity. Figures 3-5 illustrate the nature of interactions among the eddies which are identified with "B" and "C" in equation (25). The large-eddy/large-eddy interaction in the

P_1 equation [which is the real part of equation (12)] is used as an illustrative example and is shown for three sets of wave numbers, 0.2, 0.5, and 1.0 (1/cm), in Fig. 3. It is found that the values of "B" in equation (25) for wave numbers the same as or less than 0.2 (1/cm) are predominantly negative in the inner part of the boundary layer. A negative value of "B" refers to an energy supply and a positive value, an energy drain because the value of P_1 itself in the inner layer is negative for those wave numbers. The profiles of the nonlinear term show both types of behavior at the wave number about 0.5 (1/cm) and positive behavior at higher wave numbers than 0.5 (1/cm). Thus, the nonlinear eddy-eddy interactions for lower wave numbers cause energy gain while that for higher wave numbers dissipates the energy.

Shown in Figs. 4 and 5 are comparisons between "B" and "C" terms in equation (25) for the P_1 equation. Figure 4 shows terms "B" and "C" at the low wave number $k_1 = 0.1$ (1/cm) and Fig. 5 compares the same terms at the value of $k_1 = 5.0$ (1/cm), both for a fixed value of the wave number k_3 at 0.05 (1/cm). Profiles of the P_1 are also provided in the two figures to indicate their behavior in y at the same wave numbers. An opposite sign in "B" or "C" from that of P_1 implies energy loss and the same sign implies energy gain. The value of $k_3 = 0.05$ (1/cm) was chosen in these illustrations because it emphasizes the differences occurring in the alternatives of k_1. Similar results are expected of "B" and "C" for other values of k_3 when k_1 is varied in the same manner. Figure 4 shows that at the same wave number ($k_1 = 0.1$) and $y/d = 0.5$, the turbulent energy transfer because of the first mode self-interactions is much smaller than that caused by the rest of the modes when the latter are modeled with ν_T = constant. If other models were employed for the eddy-eddy interactions, this emphasis on energy loss could be reduced. The magnitude of the higher mode-interactions exceeds that of the first mode self-interactions considerably in both Figs. 4 and 5 to dissipate the energy gained not only from the large eddy but also from the mean flow [term "A," equation (25)]. Again from the signs of P_1, "B", and "C" in Figs. 4 and 5, one can infer that the higher modes interactions drain the energy consistently for all wave numbers, while large eddy self-interactions either supply energy for lower wave numbers or subtract it for higher wave numbers. Study of these figures illustrates that the influence of the eddy-viscosity model for the higher modes interactions is dominant and suggests

multiple mode analysis (in conjunction with improved models for higher modes interactions) is necessary to capture the nonlinear process properly.

5.3 Reynolds Stresses

From the deterministic large-eddy spectra, P_1 through P_8, Reynolds stress components have been obtained from equation (20). In Figs. 6 and 7, the Reynolds stresses obtained as a function of (y,t) are given for $\overline{u^2}$ and $\overline{v^2}$ only at every 25 time steps to show the development in time. The solution adjusts itself quickly in time and the effect of the initial conditions appears to be minimal. To see whether the Reynolds stresses in Figs. 6 and 7 change their profiles, the u and v profiles at $t = 0.15$, 0.175, and 0.2 are compared in Fig. 8 as a function of y/d. It shows that the u and v component intensities have indeed achieved an equilibrium profile for $t > 0.15$. The same observation has been made for other Reynolds stress components.

For detailed comparison, the Reynolds stresses are given as a function of y/d at time $t = 0.2$ in Fig. 9 along with experimental distributions taken from Laufer [22]. The first mode contributes approximately 30% of the observed intensities, although the shape agrees in general trend with the experimental distribution. In case of the w component, the use of the isotropic viscosity has caused spuriously higher proportion of the calculated w component than the u or v component in the contribution to the energy.

5.4 Structural Quantities

The single-point structural quantities defined in Section 3 are calculated from the Reynolds stresses and are compared with corresponding quantities obtained from measurements of Laufer [22]. In spite of low intensity levels of the large eddy as shown in Fig. 9, the normalized structural quantities in Fig. 10(a-d) agree well with the corresponding experimental quantities except for the anisotropy of the flow in the outer part of the boundary layer shown in Fig. 10(d). It is believed that this latter result is the consequence of the imposed symmetry at the channel centerline, that is, $v = 0$.

6 Concluding Remarks

Since the current paper deals only with the first mode and the balance regarding the first mode's origin, maintenance, and destruction, the question as to the number of modes in the series required to represent the turbulence field accurately to predict engineering quantities still remains unanswered.

However, the first mode is shown to be so significant that it supplies about 30% of turbulent kinetic energy and possesses a structural character that closely matches the experimental trends of the entire turbulence field.

When the turbulent transport is truncated to only the interactions between the components of the first mode, it is found that the drain of energy through the first mode is insufficient to balance the energy gain from the mean motion. Thus, the nonlinear interactions of higher modes are necessary in the dynamics of the first mode. However, the constant eddy viscosity used in the current closure is inadequate. For the improvement of the closure with respect to the higher modes interactions, it appears to be necessary to solve the first few modes simultaneously and to model the interactions from the rest of the modes. In that case, the difference between the first few modes in the role of forming a complete flow should become clear and this should answer the earlier question of the number of modes essential for the flow. The anisotropy in the interactions involving the higher modes will also decrease since the higher modes are expected to be more isotropic than the lower modes.

Acknowledgments

The research was conducted while the first author (SKH) held an NRC Research Associateship at the NASA Ames Research Center. Grateful acknowledgment is made for this support.

References

1 Cebeci, T., and Smith, A. M. O., Analysis of Turbulent Boundary Layers, Academic Press, New York, 1974.

2 Jones, W. P., and Launder, B. E., "The Prediction of Laminarization with a Two-Equation Model of Turbulence," Int. J. Heat Mass Transfer, Vol. 15, 1972, pp. 301-314.

3 Saffman, P. G., "A Model for Inhomogeneous Turbulent Flows," Proc. Roy. Soc., London, Vol. A317, No. 1530, 1970, pp. 417-433.

4 Hanjalic, K., and Launder, B. E., "A Reynolds Stress Model of Turbulence and Its Application to Thin Shear Flows," J. Fluid Mech., Vol. 52, Part 4, 1972, pp. 609-638.

5 Mellor, G. L., and Herring, H. J., "A Survey of the Mean Turbulent Field Closure Models," AIAA J., Vol. 11, No. 5, May 1973, pp. 590-599.

6 Loeve, M., Probability Theory, 2nd Edition, D. Van Nostrand Co., 1960, pp. 477-480.

7 Lumley, J. L., "The Structure of Inhomogeneous Flows," Atmospheric Turbulence and Radio Wave Propagation, eds. Yaglom, A. M. and Tartarsky, V. I., Publishing House «NAUKA», Moscow, 1967, pp. 166-176.

8 Hong, S. K., "Large Eddy Interactions in Curved Wall Boundary Layers-Model and Implications," Ph.D. Thesis, Purdue University, Indiana, 1983.

9 Hong, S. K., and Murthy, S. N. B., "Structure of Turbulence in Curved Wall Boundary Layers," AIAA-83-0457, 1983.

10 Hong, S. K., and Murthy, S. N. B., "On Effective Velocity of Transport in Curved Wall Boundary Layers," AIAA-84-0177, 1984a.

11 Hong, S. K., and Murthy, S. N. B., "Pressure-Strain Correlations in Curved Wall Boundary Layers," AIAA-84-1671, 1984b.

12 Bakewell, H. P., and Lumley, J. L., "Viscous Sublayer and Adjacent Wall Region in Turbulent Pipe Flow," Phys. Fluids, Vol. 10, 1967, pp. 1880-1889.

13 Payne, F. R., and Lumley, J. L., "Large Eddy Structure of the Turbulent Wake Behind a Circular Cylinder," Phys. Fluids, Vol. 10, 1967, pp. S194-S196.

14 Lemmerman, L. A., and Payne, F. R., "Extraction of the Large Eddy Structure of a Turbulent Boundary Layer," AIAA Paper 77-717, 1977.

15 Moin, P., "Probing Turbulence via Large Eddy Simulation," AIAA-84-0174, 1984.

16 Moin, P., and Kim, J., "Numerical Investigation of Turbulent Channel Flow," Vol. 118, 1982, pp. 341-377.

17 Lumley, J. L., "Coherent Structures in Turbulence," Transition and Turbulence, ed. Meyer, R. E., Academic Press, New York, 1981, pp. 215-242.

18 Townsend, A. A., Chap. 3, The Structure of Turbulent Shear Flow, 2nd Edition, Cambridge Univ. Press, London, 1976, pp. 295-298.

19 Townsend, A. A., "The Response of Sheared Turbulence to Additional Distortion," J. Fluid Mech., Vol. 81, Part 1, 1980, pp. 171-191.

20 Lumley, J. L., and Panofsky, H. A., The Structure of Atmospheric Turbulence, Interscience Pub., 1964, Appendix B, pp. 215-218.

21 Hong, S. K., "Large Eddy Interactions in Turbulent Channel Flow," to be published as NASA TM- , 1985.

22 Laufer, J., "Investigation of Turbulent Flow in a Two-Dimensional Channel," NACA Report 1053, 1951.

23 Moin, P., Reynolds, W. C., and Ferziger, J. H., "Large Eddy Simulation of Incompressible Turbulent Channel Flow," Technical Report No. TF-12, Dept. of Mech. Eng., Stanford University, 1978.

24 Greenspan, D., Discrete Numerical Methods in Physics and Engineering, Academic Press, New York, 1974, pp. 250-254.

25 Murphy, J. D., and Rubesin, M. W., "A Navier-Stokes Fast Solver for Turbulent Modeling Applications," NASA TM-78612, Aug. 1979.

Table 1 Comparison of Reynolds stresses based on two sets of parameters: S = 0.01 and ν_T = 18 (Case I); S = 0.03 and ν_T = 22 (Case II).

		$\overline{u^2}/U_o^2$		$\overline{v^2}/U_o^2$		$\overline{w^2}/U_o^2$	
J	y/H	Case I	Case II	Case I	Case II	Case I	Case II
1	Ø.ØØØØØ	Ø.ØØØØE+ØØ	Ø.ØØØØE+ØØ	Ø.ØØØØE+ØØ	Ø.ØØØØE+ØØ	Ø.ØØØØE+ØØ	Ø.ØØØØE+ØØ
2	Ø.ØØØ75	Ø.7949E-Ø5	Ø.6473E-Ø5	Ø.7Ø14E-Ø9	Ø.5776E-Ø9	Ø.6556E-Ø5	Ø.5725E-Ø5
3	Ø.ØØ15Ø	Ø.3182E-Ø4	Ø.259ØE-Ø4	Ø.1Ø87E-Ø7	Ø.8941E-Ø8	Ø.2562E-Ø4	Ø.2241E-Ø4
4	Ø.ØØ225	Ø.7135E-Ø4	Ø.5809E-Ø4	Ø.5359E-Ø7	Ø.44Ø2E-Ø7	Ø.5621E-Ø4	Ø.4926E-Ø4
5	Ø.ØØ3ØØ	Ø.1258E-Ø3	Ø.1Ø25E-Ø3	Ø.1652E-Ø6	Ø.1355E-Ø6	Ø.9723E-Ø4	Ø.854ØE-Ø4
6	Ø.ØØ375	Ø.1939E-Ø3	Ø.1582E-Ø3	Ø.393ØE-Ø6	Ø.322ØE-Ø6	Ø.1475E-Ø3	Ø.1299E-Ø3
7	Ø.ØØ475	Ø.3Ø24E-Ø3	Ø.2477E-Ø3	Ø.9767E-Ø6	Ø.7995E-Ø6	Ø.2269E-Ø3	Ø.2ØØ4E-Ø3
8	Ø.ØØ525	Ø.4905E-Ø3	Ø.4Ø54E-Ø3	Ø.2769E-Ø5	Ø.2264E-Ø5	Ø.3663E-Ø3	Ø.3254E-Ø3
9	Ø.ØØ825	Ø.78ØØE-Ø3	Ø.6523E-Ø3	Ø.7758E-Ø5	Ø.6335E-Ø5	Ø.5748E-Ø3	Ø.5146E-Ø3
1Ø	Ø.Ø1Ø75	Ø.1159E-Ø2	Ø.9853E-Ø3	Ø.1979E-Ø4	Ø.162ØE-Ø4	Ø.8358E-Ø3	Ø.7598E-Ø3
11	Ø.Ø15ØØ	Ø.17Ø7E-Ø2	Ø.15Ø2E-Ø2	Ø.5910E-Ø4	Ø.488ØE-Ø4	Ø.12Ø2E-Ø2	Ø.1123E-Ø2
12	Ø.Ø2ØØØ	Ø.2Ø69E-Ø2	Ø.1894E-Ø2	Ø.1287E-Ø3	Ø.1Ø88E-Ø3	Ø.1442E-Ø2	Ø.1387E-Ø2
13	Ø.Ø25ØØ	Ø.2186E-Ø2	Ø.2Ø62E-Ø2	Ø.2Ø7ØE-Ø3	Ø.1795E-Ø3	Ø.1533E-Ø2	Ø.15Ø1E-Ø2
14	Ø.Ø35ØØ	Ø.2Ø71E-Ø2	Ø.2ØØØE-Ø2	Ø.34Ø1E-Ø3	Ø.3118E-Ø3	Ø.1495E-Ø2	Ø.1475E-Ø2
15	Ø.Ø45ØØ	Ø.1913E-Ø2	Ø.1847E-Ø2	Ø.4227E-Ø3	Ø.398ØE-Ø3	Ø.1434E-Ø2	Ø.141ØE-Ø2
16	Ø.Ø6ØØØ	Ø.17Ø9E-Ø2	Ø.1646E-Ø2	Ø.5Ø41E-Ø3	Ø.4867E-Ø3	Ø.1351E-Ø2	Ø.1319E-Ø2
17	Ø.Ø75ØØ	Ø.1552E-Ø2	Ø.1494E-Ø2	Ø.5341E-Ø3	Ø.5172E-Ø3	Ø.1288E-Ø2	Ø.1255E-Ø2
18	Ø.Ø9ØØØ	Ø.1435E-Ø2	Ø.1387E-Ø2	Ø.5465E-Ø3	Ø.53Ø2E-Ø3	Ø.1232E-Ø2	Ø.1199E-Ø2
19	Ø.1Ø5ØØ	Ø.135ØE-Ø2	Ø.1311E-Ø2	Ø.5363E-Ø3	Ø.5195E-Ø3	Ø.1182E-Ø2	Ø.1149E-Ø2
2Ø	Ø.125ØØ	Ø.1265E-Ø2	Ø.1237E-Ø2	Ø.5227E-Ø3	Ø.5Ø82E-Ø3	Ø.1121E-Ø2	Ø.1Ø88E-Ø2
21	Ø.15ØØØ	Ø.12ØØE-Ø2	Ø.118ØE-Ø2	Ø.4922E-Ø3	Ø.4795E-Ø3	Ø.1Ø55E-Ø2	Ø.1Ø25E-Ø2
22	Ø.175ØØ	Ø.1144E-Ø2	Ø.113ØE-Ø2	Ø.4731E-Ø3	Ø.4634E-Ø3	Ø.9998E-Ø3	Ø.9736E-Ø3
23	Ø.2ØØØØ	Ø.1112E-Ø2	Ø.11Ø1E-Ø2	Ø.4420E-Ø3	Ø.434ØE-Ø3	Ø.9494E-Ø3	Ø.9286E-Ø3
24	Ø.225ØØ	Ø.1Ø78E-Ø2	Ø.1Ø69E-Ø2	Ø.4175E-Ø3	Ø.4111E-Ø3	Ø.9Ø91E-Ø3	Ø.8948E-Ø3
25	Ø.25ØØØ	Ø.1Ø56E-Ø2	Ø.1Ø48E-Ø2	Ø.3783E-Ø3	Ø.3736E-Ø3	Ø.858ØE-Ø3	Ø.8615E-Ø3
26	Ø.275ØØ	Ø.1Ø3ØE-Ø2	Ø.1Ø24E-Ø2	Ø.3465E-Ø3	Ø.3432E-Ø3	Ø.8393E-Ø3	Ø.841ØE-Ø3
27	Ø.3ØØØØ	Ø.1Ø1ØE-Ø2	Ø.1ØØ7E-Ø2	Ø.2989E-Ø3	Ø.2977E-Ø3	Ø.8Ø55E-Ø3	Ø.8166E-Ø3
28	Ø.325ØØ	Ø.9878E-Ø3	Ø.9872E-Ø3	Ø.2613E-Ø3	Ø.2615E-Ø3	Ø.7885E-Ø3	Ø.8Ø87E-Ø3
29	Ø.35ØØØ	Ø.9586E-Ø3	Ø.9614E-Ø3	Ø.2Ø79E-Ø3	Ø.21ØØE-Ø3	Ø.75ØØE-Ø3	Ø.79ØØE-Ø3
3Ø	Ø.375ØØ	Ø.9436E-Ø3	Ø.9493E-Ø3	Ø.1678E-Ø3	Ø.17Ø3E-Ø3	Ø.7544E-Ø3	Ø.7921E-Ø3
31	Ø.4ØØØØ	Ø.9292E-Ø3	Ø.9384E-Ø3	Ø.1145E-Ø3	Ø.1179E-Ø3	Ø.7333E-Ø3	Ø.7798E-Ø3
32	Ø.425ØØ	Ø.9247E-Ø3	Ø.9367E-Ø3	Ø.7828E-Ø4	Ø.8Ø64E-Ø4	Ø.7437E-Ø3	Ø.797ØE-Ø3
33	Ø.45ØØØ	Ø.9177E-Ø3	Ø.9335E-Ø3	Ø.3589E-Ø4	Ø.3781E-Ø4	Ø.7313E-Ø3	Ø.793ØE-Ø3
34	Ø.475ØØ	Ø.9342E-Ø3	Ø.9527E-Ø3	Ø.1348E-Ø4	Ø.1376E-Ø4	Ø.7639E-Ø3	Ø.8316E-Ø3
35	Ø.5ØØØØ	Ø.9435E-Ø3	Ø.9651E-Ø3	Ø.ØØØØE+ØØ	Ø.ØØØØE+ØØ	Ø.7776E-Ø3	Ø.8544E-Ø3

J = sequence

Y = distance from wall

H = channel width

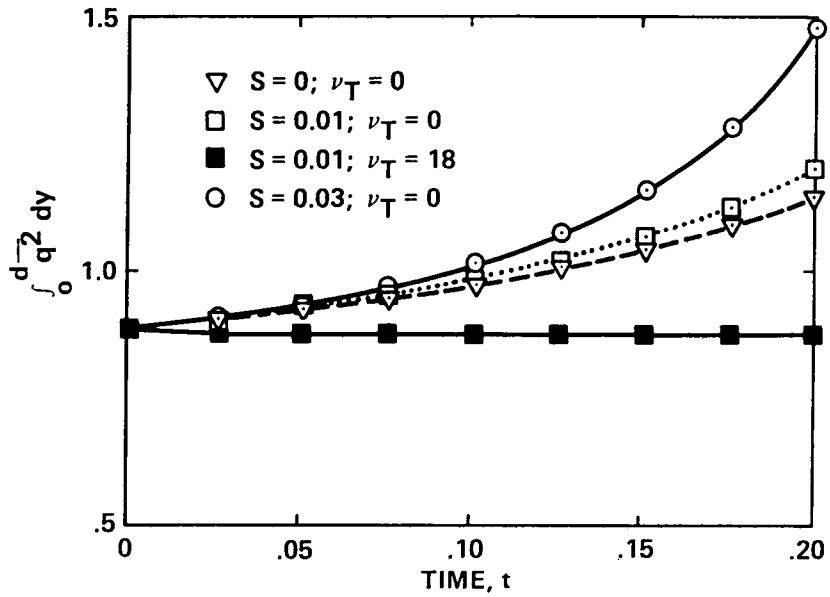

Fig. 1 Turbulent kinetic energy versus t for various values of skewness parameter, S

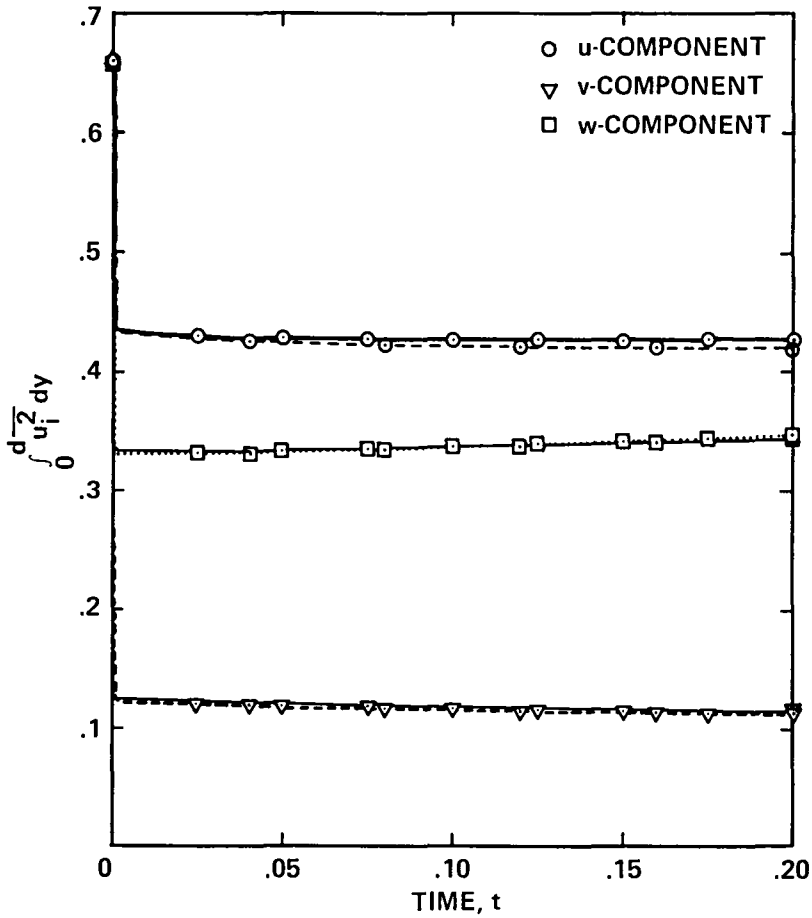

Fig. 2 Turbulent energy growth in time among three components for two sets of parameters: solid line for (S = 0.01, ν_T = 18); dashed line for (S = 0.03, ν_T = 22)

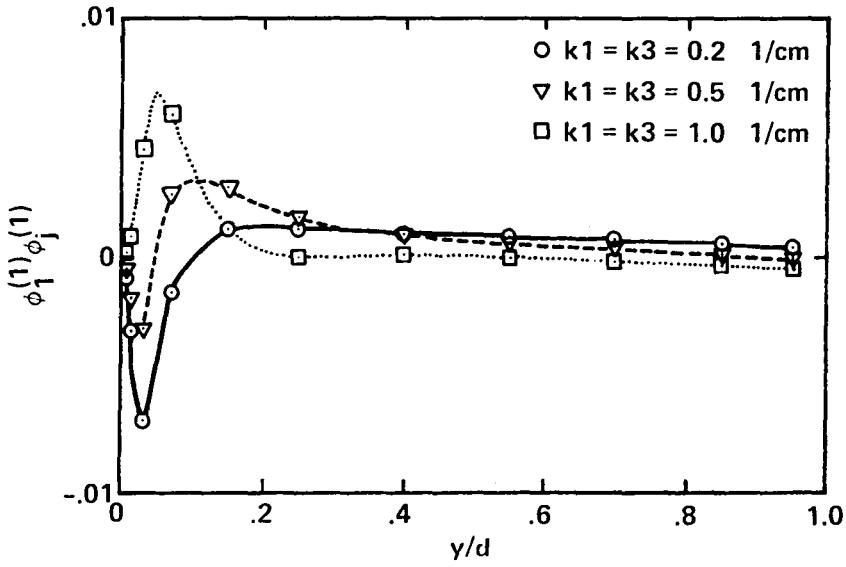

Fig. 3 Profiles of $S(\partial/\partial x_j)\{(\lambda_1\phi_1^{(1)})(\lambda_1\phi_j^{(1)})\}$ versus y/d for various wave numbers at t = 0.2

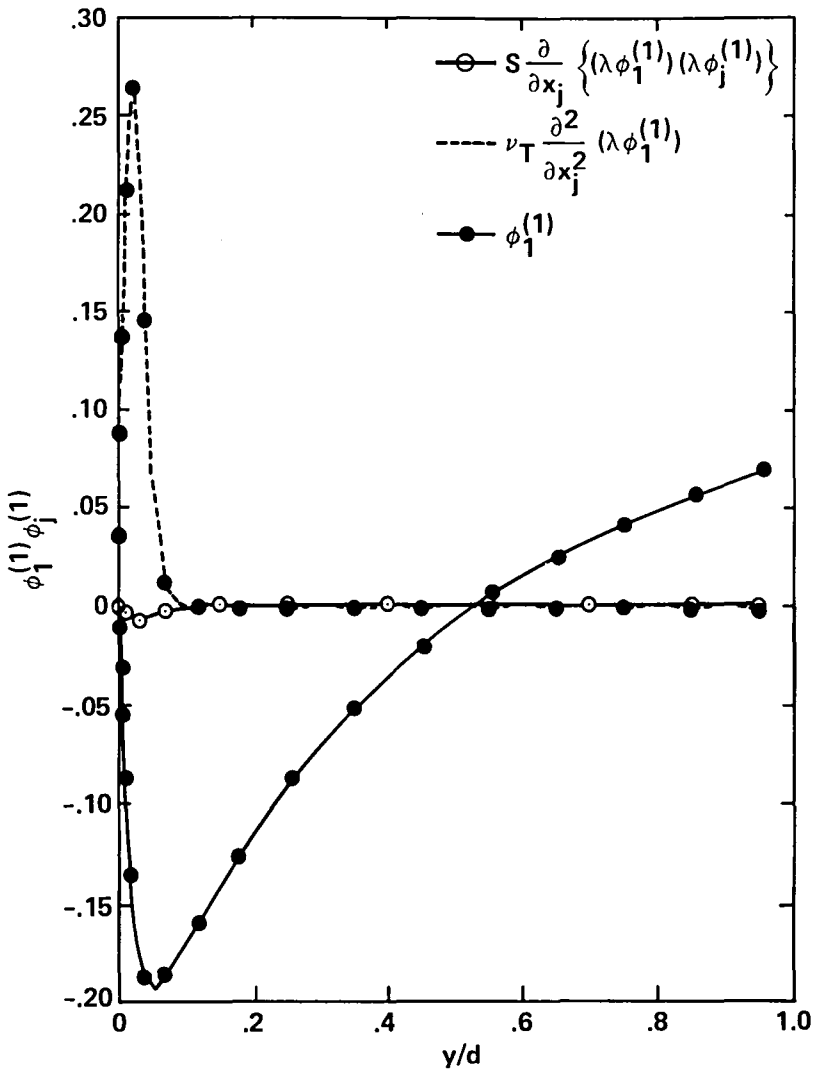

Fig. 4 Profiles of large eddy self-interactions and modeled higher modes interactions versus y/d for $k_1 = 0.1$ and $k_3 = 0.05$ (1/cm) at $t = 0.2$

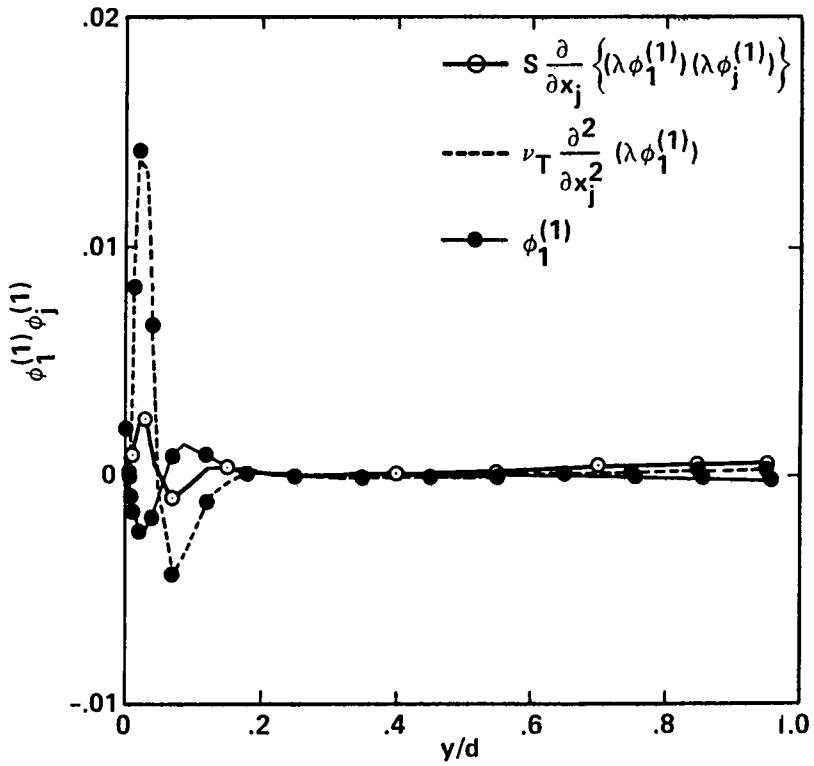

Fig. 5 Profiles of large eddy self-interactions and modeled higher modes interactions versus y/d for k_1 = 5.0 and k_3 = 0.05 (1/cm) at t = 0.2

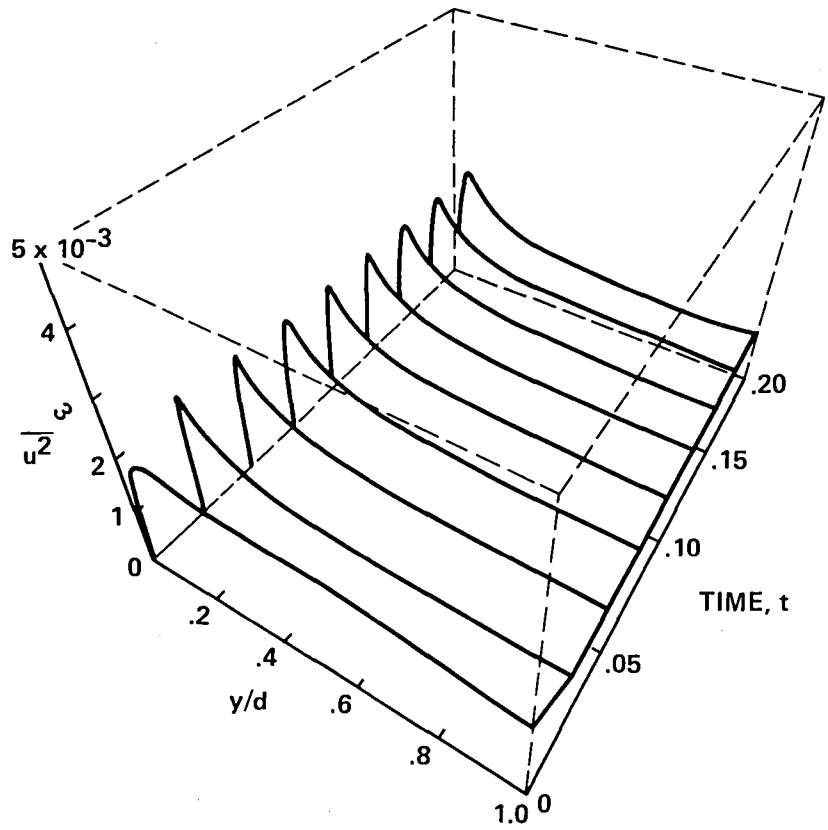

Fig. 6 Development of streamwise turbulent intensity ($\overline{u^2}/U_o^2$) in (y,t)

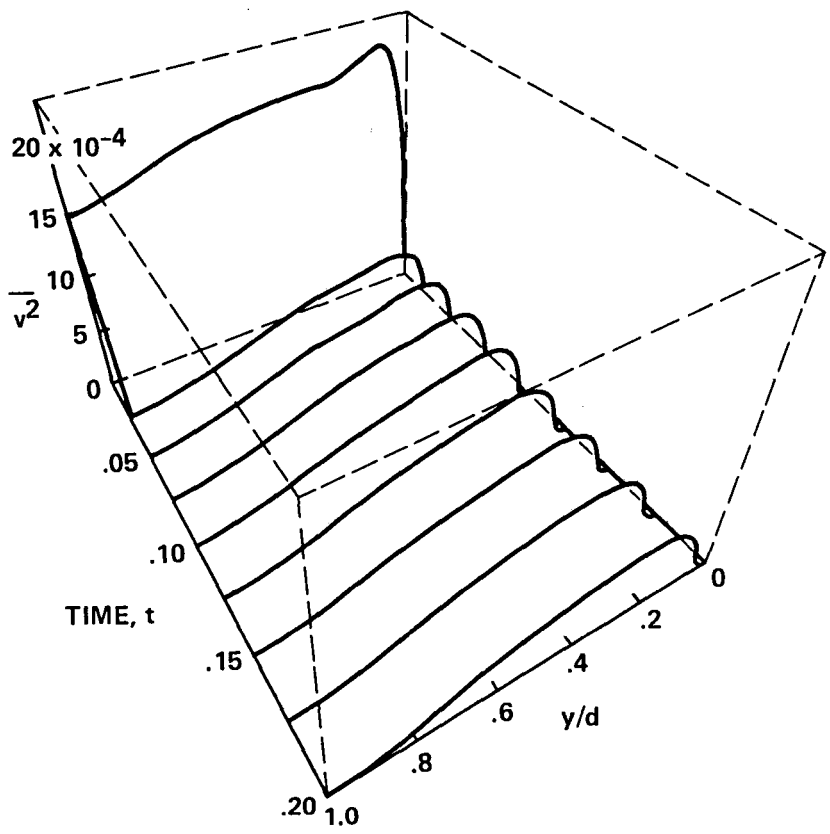

Fig. 7 Development of normal turbulent intensity ($\overline{v^2}/U_o^2$) in (y,t) space

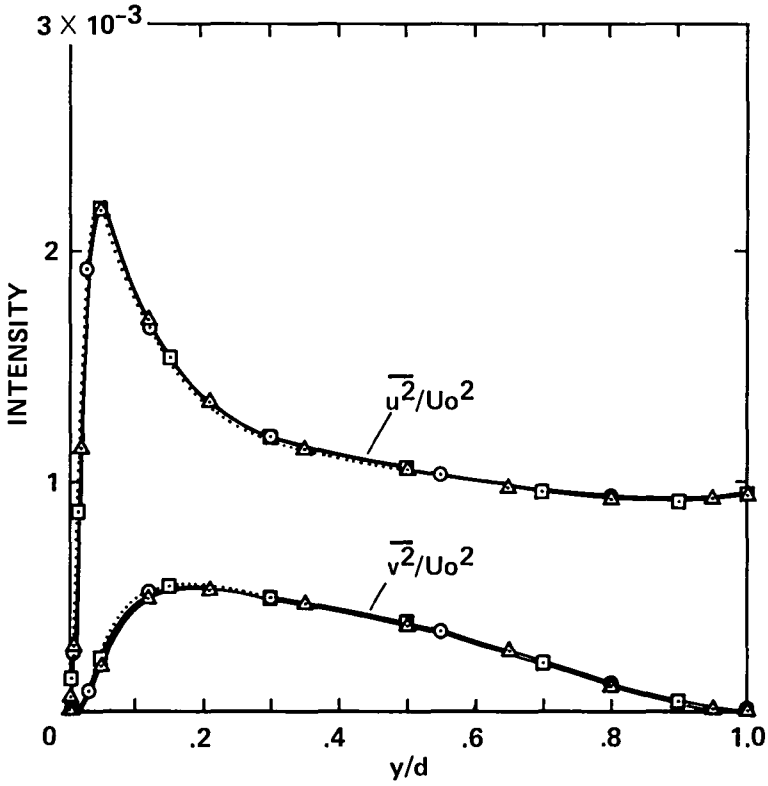

Fig. 8 Comparison of three $\overline{u^2}$ and $\overline{v^2}$ profiles at t = 0.15 (o), 0.175 (×), and 0.2 (△)

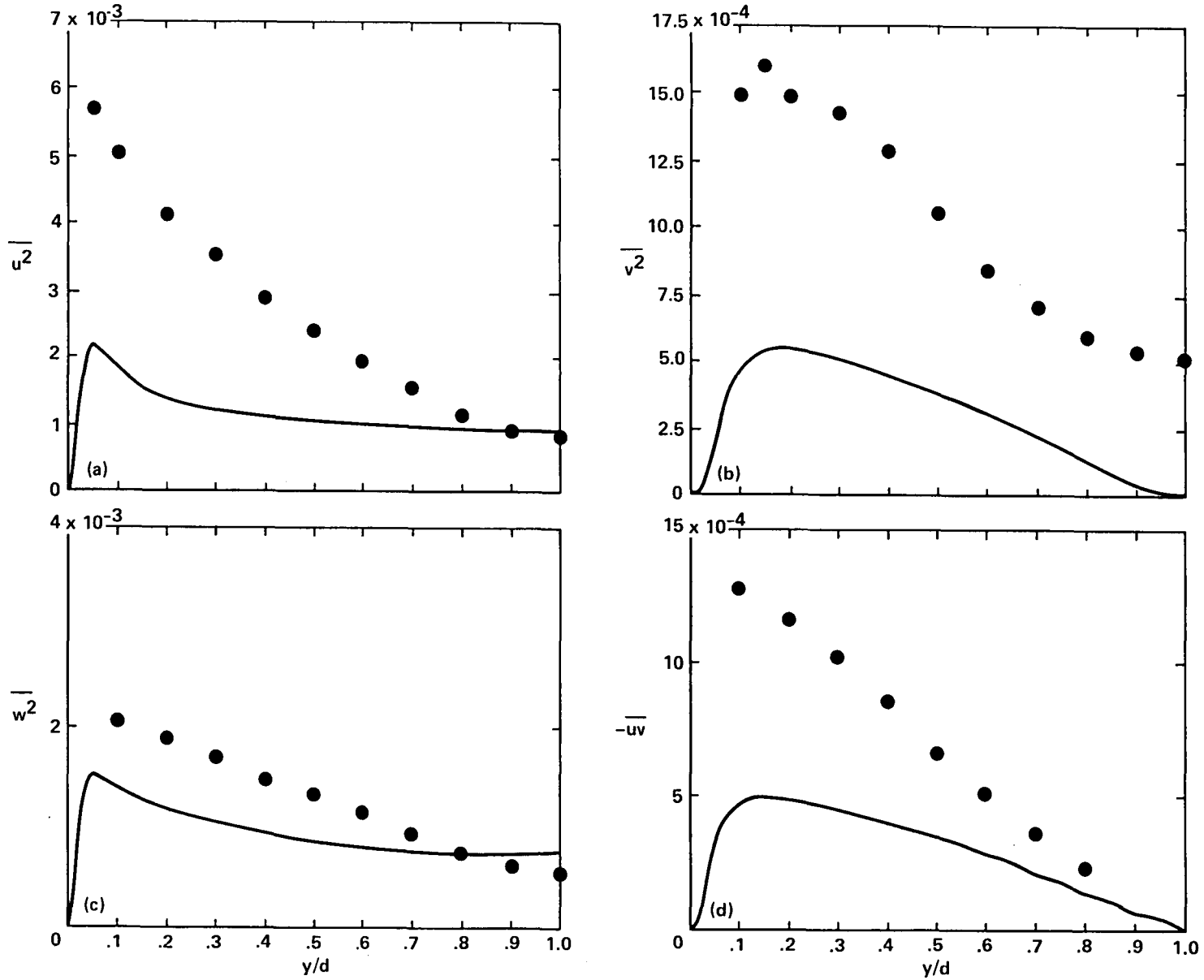

Fig. 9 Contribution from the first mode to (a) $\overline{u^2}$, (b) $\overline{v^2}$, (c) $\overline{w^2}$, and (d) $\overline{uv}$, divided by U_o^2, versus y/d at t = 0.2: ●● Laufer [22]

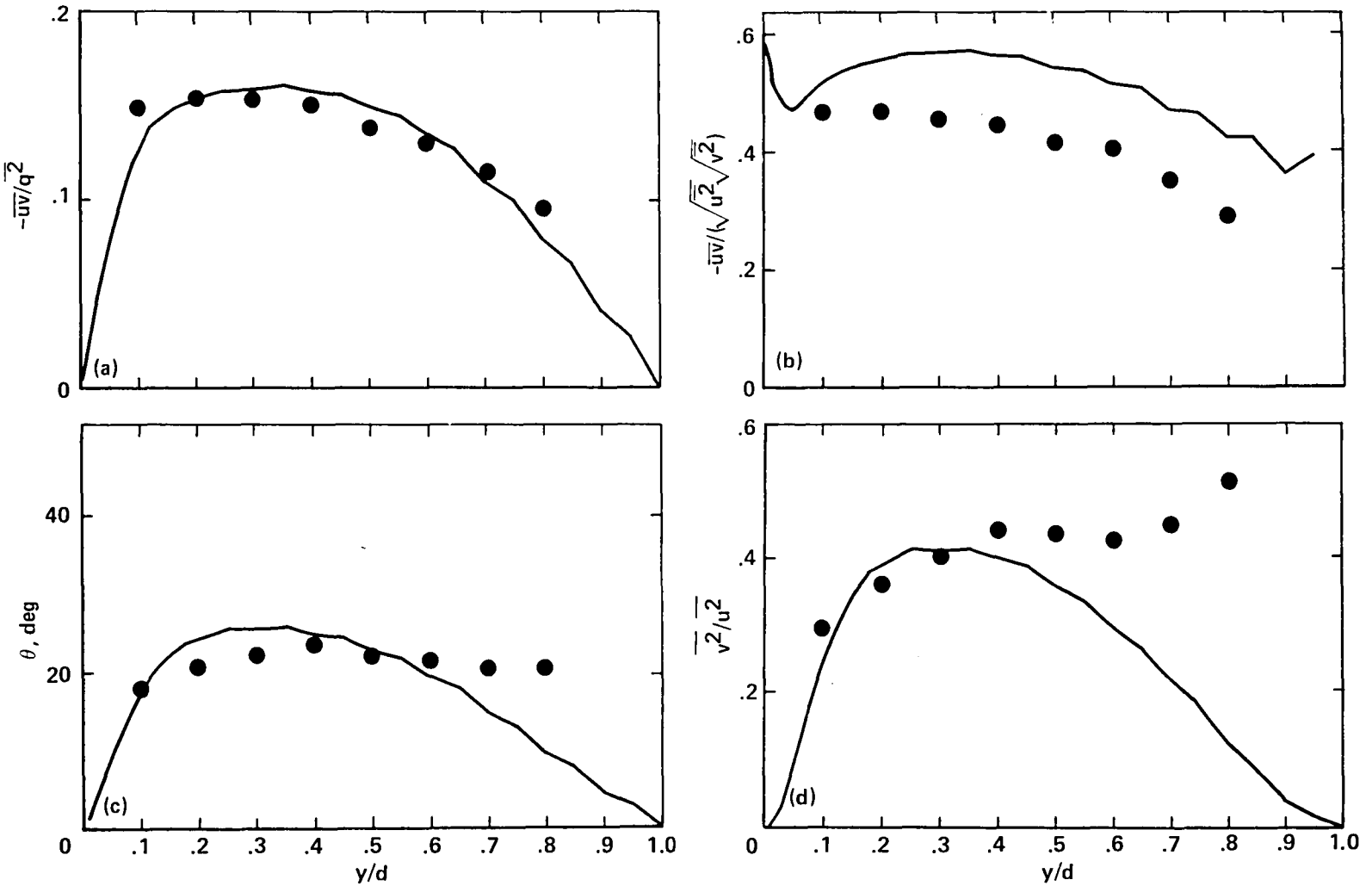

Fig. 10 Structural quantities calculated from the first mode versus y/d at t = 0.2: ●● Laufer [22]; (a) $\overline{uv}/\overline{q^2}$, (b) $\overline{uv}/\sqrt{\overline{u^2}}\sqrt{\overline{v^2}}$, (c) θ in equation (21), and (d) $\overline{v^2}/\overline{u^2}$

1. Report No.	2. Government Accession No.	3. Recipient's Catalog No.
NASA TM-86691		

4. Title and Subtitle	5. Report Date
APPLICATION OF LARGE-EDDY INTERACTION MODEL TO CHANNEL FLOW	February 1985
	6. Performing Organization Code
7. Author(s)	8. Performing Organization Report No.
S. K. Hong and M. W. Rubesin	85148
	10. Work Unit No.
9. Performing Organization Name and Address	T6459
Ames Research Center Moffett Field, CA 94035	11. Contract or Grant No.
	13. Type of Report and Period Covered
12. Sponsoring Agency Name and Address	Technical Memorandum
National Aeronautics and Space Administration Washington, DC 20546	14. Sponsoring Agency Code 506-51-11

15. Supplementary Notes

Point of Contact: S. K. Hong, Ames Research Center, MS 229-1, Moffett Field, CA 94035 (408) 694-6229 or FTS 464-6229

16. Abstract

A procedure utilizing an expansion of proper orthogonal functions (or modes) to predict a fully developed flow in channel is derived. To examine numerical and conceptual difficulties, preliminary computations are performed with assigned mean velocity, and turbulence is expressed with only the first mode. The nonlinear interactions of the components of the first mode are treated specifically, with the influence of higher modes neglected; this treatment required adjustment of the skewness and effective Reynolds number to assure energy equilibrium of the first mode. Computational results show that the first mode possesses the structural character similar to that of the entire flow.

17. Key Words (Suggested by Author(s))	18. Distribution Statement
Large eddy Proper orthogonal expansion Channel flow Reynolds stress Turbulence structure	Unlimited Subject Category - 34

19. Security Classif. (of this report)	20. Security Classif. (of this page)	21. No. of Pages	22. Price*
Unclassified	Unclassified	32	A03

*For sale by the National Technical Information Service, Springfield, Virginia 22161

End of Document